Finite Element Modelling of Reinforced Concrete Beams with Corroded Shear Reinforcement

S. Bernard, B. Martín-Pérez
Department of Civil Engineering, University of Ottawa, Ottawa, Ontario, Canada

Abstract: This paper presents a finite element modelling approach of shear critical reinforced concrete (RC) beams with corroded shear reinforcement. Shear reinforcement was modelled using a "locally smeared" approach, wherein the shear reinforcement is smeared within a series of plane-stress concrete elements at the specific stirrup location. This was done with the objective of incorporating both the reduction in cross-sectional area due to corrosion and the corresponding expansion of corrosion products build up. To determine the strain induced by the corrosion products in the affected surrounding concrete, the concrete cover was treated as a thick-wall cylinder subjected to internal pressure. These strains were introduced in the finite element model using fictitious smeared horizontal pre-stressing steel, with a compressive pre-straining level related to the degree of corrosion necessary to induce cracking. The finite element modelling approach was validated against published test data of shear critical RC beams with and without stirrup corrosion. The proposed modelling approach successfully reproduces the load-deformation response as well as the failure mode and cracking patterns of the published experimental tests.

1. Introduction

Much of the Canadian reinforced concrete (RC) infrastructure is exposed to the application of de-icing salts in the winter in addition to repetitive cycles of freezing and thawing action. This harsh environment in combination with poor construction practice, a lack in detailing and little or no maintenance work, often lead to an early onset of reinforcement steel corrosion, causing these structures not to reach the end of their design life. Out of all the possible sources of deterioration for concrete, reinforcement corrosion has been shown to be the most severe and extended (Hanjari et al. 2011). Since shear reinforcement is protected by a lower concrete cover than longitudinal reinforcement, it is likely that under the described conditions, stirrups will start corroding first. The pitting corrosion in the stirrups in addition to the corresponding cracking/spalling of the concrete cover on the compression side of RC beams are factors that may lead to a premature shear failure. Given the large amount of structures affected, it is imperative to develop tools to assess the consequences of this deterioration on the shear capacity of RC flexural members. In order to assess the structural consequences of the observed damage, it is required to quantify both the stiffness and strength of affected RC members in the deteriorated state.

This paper presents a finite element modelling approach to study the effect of corroded shear reinforcement on the behaviour and strength of shear critical RC beams. The finite element model accounts for both the reduction in cross-sectional area of the stirrups as well as corrosion-induced cracking of the surrounding concrete cover. The finite element modelling approach is further validated against experimental tests of corrosion-affected shear critical RC beams published in the literature.

2. Finite Element Model

Finite element modelling to study the effect of shear reinforcement corrosion on the shear capacity of RC beams was conducted using the nonlinear finite element package VecTor2 (Wong and Vecchio 2002). The following sections describe the finite elements used as well as some considerations to be accounted for in the modelling of shear critical RC beams.

2.1 Finite Element Mesh

Plain concrete elements were modelled using a 4-node rectangular plane stress element, with 2 degrees of freedom at each node, as shown in Figure 1.

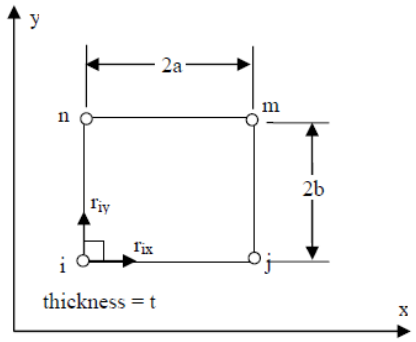

Figure 1: Four-node plane stress element (reproduced from Wong and Vecchio 2002)

For regions where shear reinforcement is well distributed and assumed to be smeared across the element, the material matrix for the plane stress element $[D]$ is modified to account for both the concrete $[D_c]$ and steel $[D_s]$ contributions as follows:

[1] $$[D]=[D_c]+\sum_{i=1}^{n}[D_s]_i$$

The concrete material matrix $[D_c]$ is defined for a given load stage as:

[2] $$[D_c]' = \begin{bmatrix} \bar{E}_{c1} & 0 & 0 \\ 0 & \bar{E}_{c2} & 0 \\ 0 & 0 & \bar{G}_c \end{bmatrix}$$

where $\bar{E}_{c1}$ is the modulus of elasticity for concrete in the primary direction, $\bar{E}_{c2}$ is the modulus of elasticity for concrete in the secondary direction, and $\bar{G}_c$ is the shear modulus. Equation 2 models concrete as an orthotropic material along the principal directions (Wong and Vecchio 2002). The $[D_s]_i$ matrix in Eq. 1 describes the steel contribution along the i^{th} direction and for a given load stage is defined as follows:

[3] $$[D_s]_i' = \begin{bmatrix} \rho_i \bar{E}_{si} & 0 & 0 \\ 0 & 0 & 0 \\ 0 & 0 & 0 \end{bmatrix}$$

where $\bar{E}_{si}$ is the modulus of elasticity of the steel in the i^{th} direction, and ρ_i is the percentage of steel distributed within the element along the same direction. The stresses in the reinforced concrete element $\{\sigma\}$ are related to the total strains $\{\varepsilon\}$ through the composite material stiffness matrix $[D]$ as follows:

[4] $$\{\sigma\} = [D]\{\varepsilon\} - \{\sigma^o\}$$

where $\{\sigma^o\}$ represents the stress contribution of strain offsets and shear slip strains (Wong and Vecchio 2002). This stress vector $\{\sigma^o\}$ is obtained from Eq. 5, i.e.,

[5] $$\{\sigma^o\} = [D_c]\left(\{\varepsilon_c^o\} + \{\varepsilon_c^p\} + \{\varepsilon^s\}\right) + \sum_{i=1}^{n}[D_s]_i\left(\{\varepsilon_s^o\}_i + \{\varepsilon_s^p\}_i\right)$$

Where $\{\varepsilon_c^o\}$ is the concrete elastic strain offset (due to thermal, prestrains, shrinkage and lateral expansion effects), $\{\varepsilon_c^p\}$ is the concrete plastic strain offset (due to cyclic loading or damage), and $\{\varepsilon^s\}$ represents the strain due to crack shear slip (Wong and Vecchio 2002). Likewise, $\{\varepsilon_s^o\}_i$ and $\{\varepsilon_s^p\}_i$ are respectively the elastic and plastic strain offsets in the i^{th} direction of the reinforcing steel.

The shear reinforcement was modelled here using rectangular plane-stress elements with the composite material matrix in Eq. 1. However, depending on where the shear reinforcement is located within the beam, two distinct modelling approaches were used. For sections that are considered non-critical in terms of stirrup corrosion, the shear reinforcement was smeared across the elements. It was incorporated as a percentage of steel reinforcement distributed equally throughout the elements in the region. For sections that are critical, wherein corrosion in the stirrup needs to be introduced, the stirrups were isolated by means of composite elements with a width equal to the stirrup diameter. This generates two types of elements within the critical section, plain unreinforced concrete elements and "locally smeared" (LS) reinforced concrete elements. This was done for two reasons. First, the properties for each stirrup can be modified independently based on the degree of corrosion. Second, a corrosion-induced cracking model, as later described, can be introduced by means of simulating the expansion caused by corrosion build up on the stirrup legs.

Compression and tension flexural reinforcement were modelled using 2-node truss elements, with one degree of freedom per node. These elements can only transfer axial loads. If corrosion is considered along the longitudinal reinforcement, the properties of the truss elements can be modified accordingly. Furthermore, truss elements also lend themselves to incorporate a bond element (e.g., a spring) within the model, if bond is chosen to be a critical factor in modeling the member's behavior.

A typical finite element mesh of an RC beam is shown in Figure 2. The light green elements at the beam's ends as well as the blue right side are modelled with composite non-critical elements, in which the shear reinforcement is smeared throughout this region based on the percentage of steel intended in the design. The left side of the beam is modelled with plain unreinforced concrete elements (light blue) and LS elements for the stirrups.

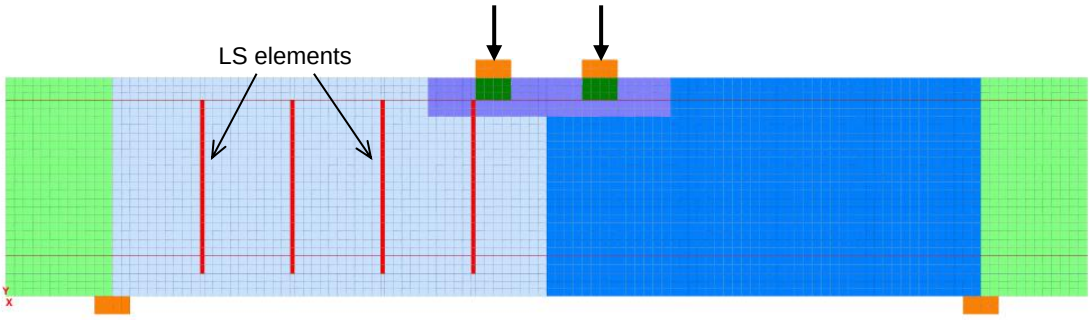

Figure 2: Typical FE meshing

2.2 Considerations in ModellingShear Critical Beams

Modeling a RC beam governed by shear is not a straightforward task as the material exhibits complex behavior under shear stresses. As a composite material, RC uses a combination of mechanisms to resist shear forces across a section depending on the amount of flexural reinforcement, span length, beam depth, and shear reinforcement present within the member. For most cases, shear forces are transferred across a section through the stirrups, the concrete compression zone, by aggregate interlock at cracks, as well as through dowel action of the longitudinal reinforcement. Depending on the geometry of the beam, loading scheme and reinforcement configuration, different failure mechanisms can develop. It is important to properly identify the probable failure mechanism and use judgement when modeling shear critical beams in order to select adequate models and acknowledge limitations in the finite element simulation.

When finite element modeling is selected, it is important to acknowledge how the program takes into account the different mechanical properties and mechanisms within the finite element framework. VecTor2 (Wong and Vecchio 2002) was chosen for the simulation, because it specialises in RC modelling and allows the user to select between a wide range of behaviour models and material limits. It uses either the Modified Compression Field Theory (MCFT) or the Disturbed Stress Field Theory (DSFT) (Vecchio 2000, Vecchio et al. 2001) for the shear strength calculation. The main difference between these shear models is in the alignment between the principal stresses and principal strains. The MCFT theory assumes that both principal stresses and strains are aligned, whereas the DSFT accounts for a lag between the two. This is interpreted in the software as a slip at the crack, where the MCFT does not account for any slip. Both models are limited by two checks done locally at a crack (Vecchio 2000). The first is by a shear stress check, where only a certain amount of stress can be transferred by aggregate interlock across the crack. The second is a crack width check, where in order for the aggregate to interlock properly, the crack width needs to be limited. Both approaches properly model shear behaviour in RC, although the DSFT depicts better the actual shear behavior of concrete as slip at a crack naturally occurs. It is for this reason that DSFT was selected here for the simulation.

3. Corrosion-Induced Cover Cracking Model

Corrosion of reinforcing steel in RC structures can be described as a time-dependent process with two stages. The first is the initiation period. Its length will depend on multiple factors such as the level of chloride contamination in the concrete cover, cover depth, rebar protection, etc. Once a threshold level of chloride is reached at the steel/concrete interface, the second phase starts by the onset of corrosion. The virgin steel then begins to transform into various types of ferrous oxides. Due to the decrease in density of these oxides compared to the virgin steel, the bar begins to increase in volume. The accumulation of rust by-products around the rebar generates a pressure on the surrounding concrete, and when the concrete tensile capacity is reached, the concrete starts to crack and releases this accumulated energy, as illustrated in Figure 3(a). Eventually this leads to visible cracks at the concrete surface, soon followed by spalling and/or delamination of the cover depending on the severity of the attack and on the configuration of the reinforcement. The concrete cover subjected to the pressure generated by the accumulation of

corrosion products around the reinforcing bar can be idealized as a thick-wall cylinder with an internal pressure p_i as illustrated Figure 3(b). Once the tensile limit on the concrete is reached at the steel/concrete interface, the concrete starts to crack and dissipates stored energy from an initial pressure p_i to an effective pressure p_e at the crack limit. It is assumed that the pressure is fully released once the crack reaches the surface of the thick-wall cylinder.

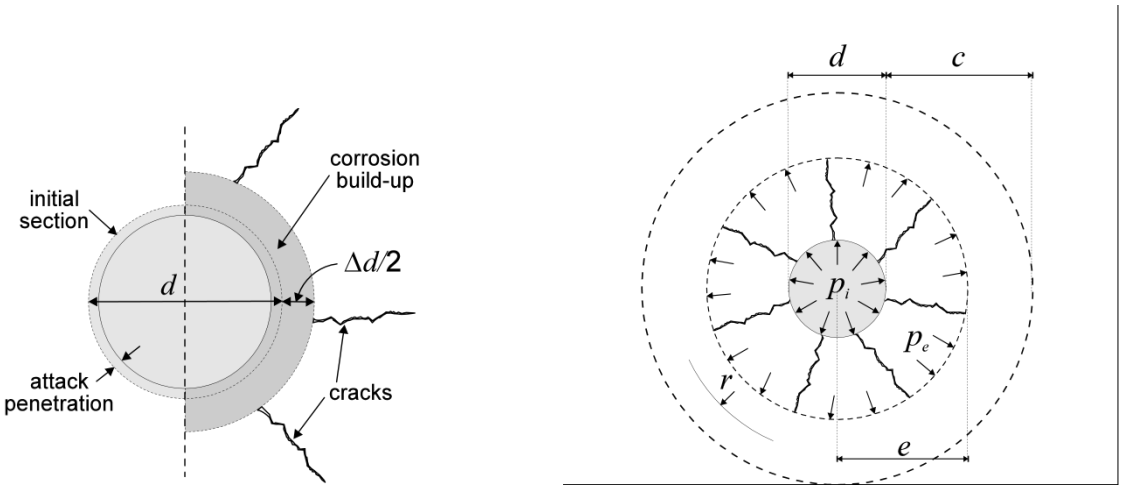

(a) (b)

Figure 3: (a) Corrosion products build up; (b) Concrete cover treated as a thick-wall cylinder subjected to internal pressure (reproduced from Martín-Pérez 1999)

In this work, corrosion-induced cracking was introduced in the finite element model by means of a compressive pre-strain within the affected elements (stirrups) to simulate the natural expansion of corrosion build up. This pre-strain acts as a spring in compression prior to the application of loading, and it is calculated based on the percentage of corrosion attack and associated volume build up. The loss of steel cross-sectional area A_{sLoss} due to corrosion is obtained from:

[6] $$A_{s\ Loss} = A_s - \frac{\pi(d-2x_{cor})^2}{4}$$

where A_s is the original cross-sectional area, d is the reinforcing steel diameter, and x_{cor} is the depth of corrosion attack penetration. The original cross-sectional area A_s is given by:

[7] $$A_s = \frac{\pi d^2}{4}$$

The total expanded area A_s' can be obtained by assuming a ratio of steel-to-corrosion product density ρ according to Eq. 8:

[8] $$A_s' = \rho A_{sLoss} + \frac{\pi\left(d-2x_{cor}\right)^2}{4}$$

The ratio ρ has been reported of having values between 2 and 4 (Rosenberg 1989). From Eq. 8, the expanded diameter d' can be easily calculated as follows:

[9] $$d' = \sqrt{\frac{4A_s'}{\pi}}$$

Finally, the strain induced in the thick wall cylinder can be calculated from:

$$[10] \qquad \varepsilon_{cor} = \frac{d' - d}{d + 2c}$$

Where ε_{cor} is the corrosion-induced strain in a single leg of the stirrup, and c is the concrete cover to the respective leg. In a two-dimensional plane-stress problem, as the one modelled here, both legs in the stirrup are assumed to be corroding, and therefore the resulting compressive pre-strain $\bar{\varepsilon}_{cor}$ is adjusted by averaging the strains in each leg over the cross section of the beam, i.e.,

$$[11] \qquad \bar{\varepsilon}_{cor} = \left(\varepsilon_{cor1} + \varepsilon_{cor2}\right) \times \left[\frac{2\left(d + 2c\right)}{b}\right]$$

where b represents the beam's width. Once the strains are calculated based on the percentage of corrosion attack, it can then be incorporated within the finite element model. This is done by smearing fictitious horizontal steel within the affected area and applying the corresponding pre-strain in compression ($\left\{\varepsilon_s^o\right\}$ in Eq. 5), so that it simulates the expansion mechanism within the surrounding concrete, eventually leading to cracking.

4. Validation Against Published Data

The finite element model described in the previous sections was validated against published data for shear critical beams without and with corrosion in the stirrups.

4.1 Test Specimens

The specimens chosen for validation were specifically designed to be shear critical and experimentally tested by Higgins et al. (2003). The beams underwent accelerated corrosion, which was focused on the shear reinforcement of the critical section of the member. A control beam (Beam 10RA) was not subjected to corrosion. The corrosion levels for the other beams ranged between low corrosion penetrations (Beam 10RB), moderate (Beam 10RC) and high levels (Beam 10RD). All the beams are denoted by 10R, as they have a rectangular section and a stirrup spacing in the critical section of 10 inches (254 mm), as shown in Figure 4. The beams were tested using a 4-point loading scheme, and the load-deflection curves recorded during the tests are shown in Figure 5. In this figure, the effects of shear reinforcement corrosion can be observed, with a decrease in both strength and mid-span deflection at ultimate load as the corrosion level increased.

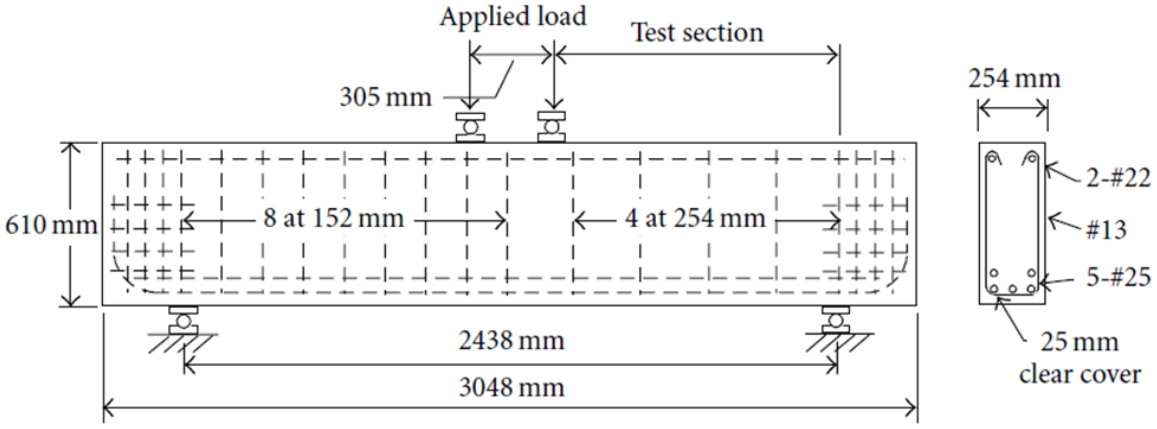

Figure 4: Test setup and member dimensions (reproduced from Miller et al. 2011)

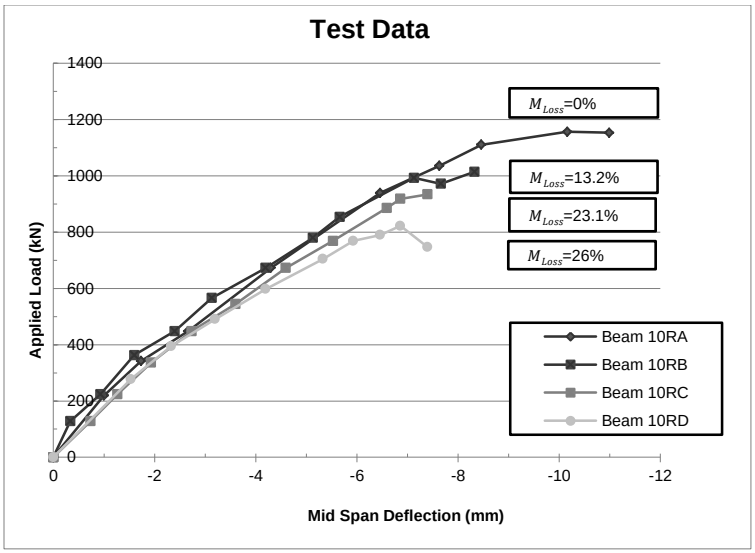

Figure 5: Load deflection for test specimens (Higgins et al. 2003)

4.2 Validation Without Corrosion in the Stirrups

Modelling the stirrups with the LS elements was validated against the control specimen (Beam 10RA) in order to see if it simulated the behaviour accurately prior to incorporating any corrosion damage. The simulations are compared against specific factors chosen to increase confidence of the proposed models. First the overall stiffness is compared to confirm general behaviour, and then the ultimate load and deflection are also compared. Finally, the failure mechanism is compared by means of identifying and comparing the failure crack patterns that were reported during the test.

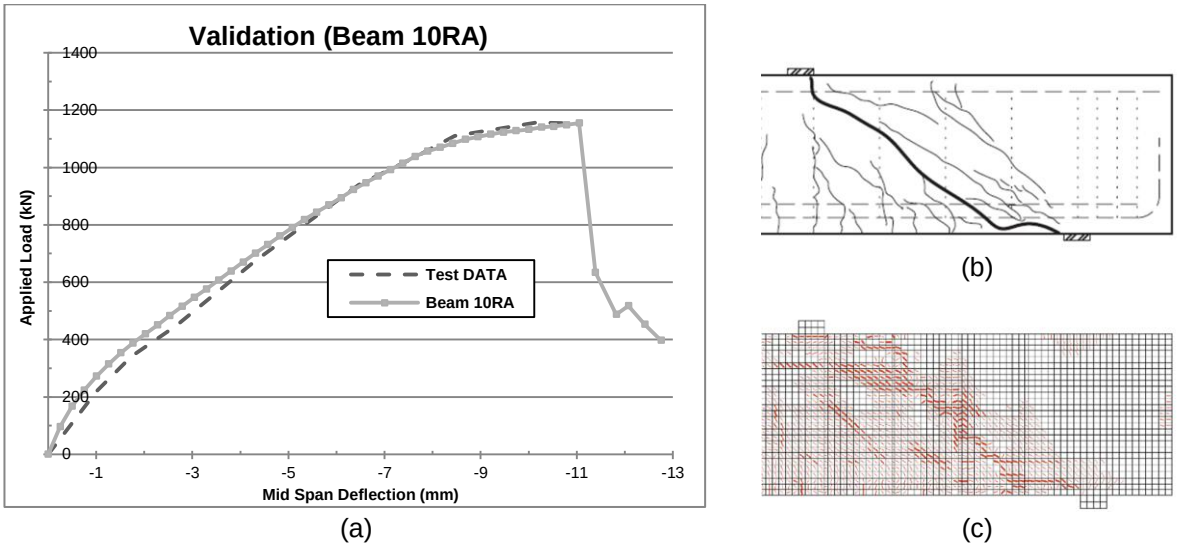

Figure 6: (a) Load-deformation for control beam; (b) Cracking map at failure for test specimen (Higgins et al. 2003); (c) Cracking generated by finite element model at failure

As it is shown in Figure 6(a), there is excellent agreement for the overall stiffness and load-deformation behavior, although the ultimate strength and deflection are slightly over estimated. Furthermore, the

modelling approach adopted simulates properly the failure mode as well as the cracking patterns at ultimate load (Figures 6(b) and 6(c)).

4.3 Validation With Corrosion in the Stirrups

For the test specimens where the stirrups were corroded, the finite element model was run when only the steel cross-sectional loss was introduced (Eq. 6) and when both the loss in steel area and corrosion-induced cracking were considered (Eq. 6 and Eq. 11). Figure 7 shows the load-deflection curve for the beam with low corrosion levels (13.2% loss). The finite element results are plotted against the test data for both with (Beam 10RBW) and without pre-straining (Beam 10RBWo). As observed in Figure 7(a), both finite element results approximate properly the load-deformation behavior. The stiffness of each model has good accuracy. Although the finite element model without pre-straining seems to better estimate ultimate strength and deflection, the one with pre-straining is a bit more conservative in its estimates. The effect of pre-straining can be noticed by a slight decrease in strength and ultimate deflection. The crack prediction of both models properly represent the actual failure mode, with the one with pre-straining having more damage as expected (Figure 7(d)).

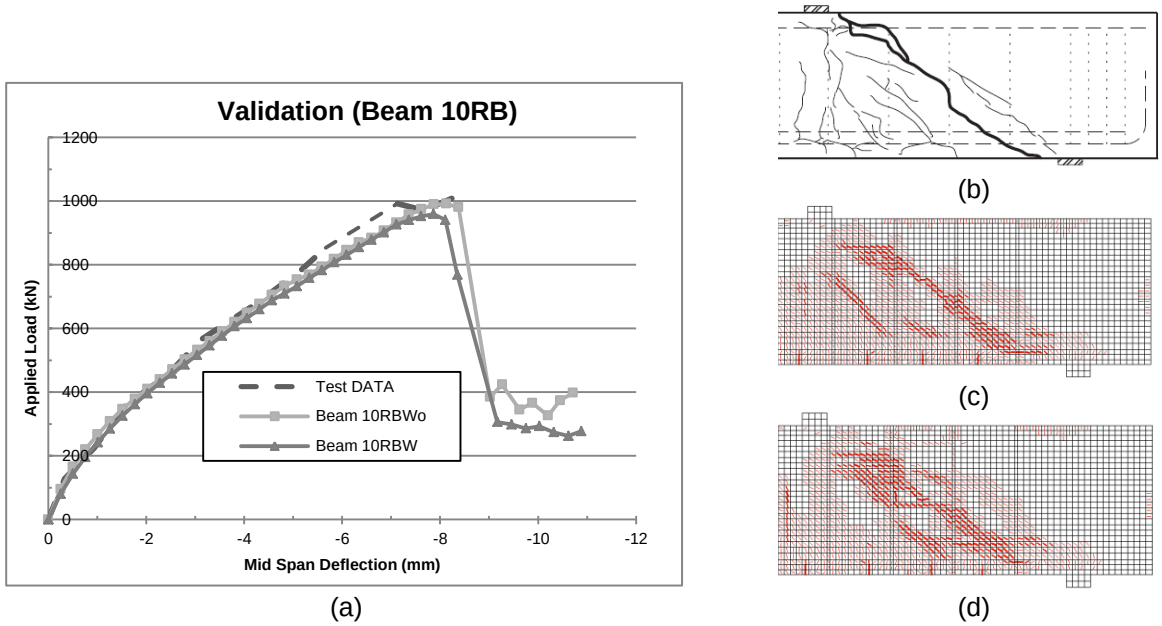

Figure 7: (a) Load-deflection for **Low** corrosion levels; (b) Crack pattern at failure for test specimen (Higgins et al. 2003); (c) Crack prediction **without** pre-straining; (d) Crack prediction **with** pre-straining

Figure 8 illustrates the results for the beam with moderate corrosion levels in the stirrups (23.1% loss). For moderate levels of corrosion, both finite element models properly simulate the stiffness, with the model with pre-straining having a slightly better estimate. Both models properly estimate ultimate strength and deflection with similar percentage of divergence, with the model that includes pre-straining being on the conservative side. Again in the cracking prediction, both models agree with the failure mode, with the pre-straining model inducing more damage and providing a slightly better approximation of the failure crack pattern.

Figure 9 shows the results for the beam with high corrosion levels in the stirrups (26% loss). At high levels of corrosion, both models have an overall stiffer behavior and a higher ultimate strength estimate than what was recorded (Figure 9(a)). The model with pre-straining has a slightly better approximation of stiffness, with a more conservative estimate of the ultimate strength. Both cracking patterns properly

simulate failure behavior, although the model with pre-straining has a better overall simulation of the failure crack pattern as well as the overall level of induced damage (Figure 9(d)).

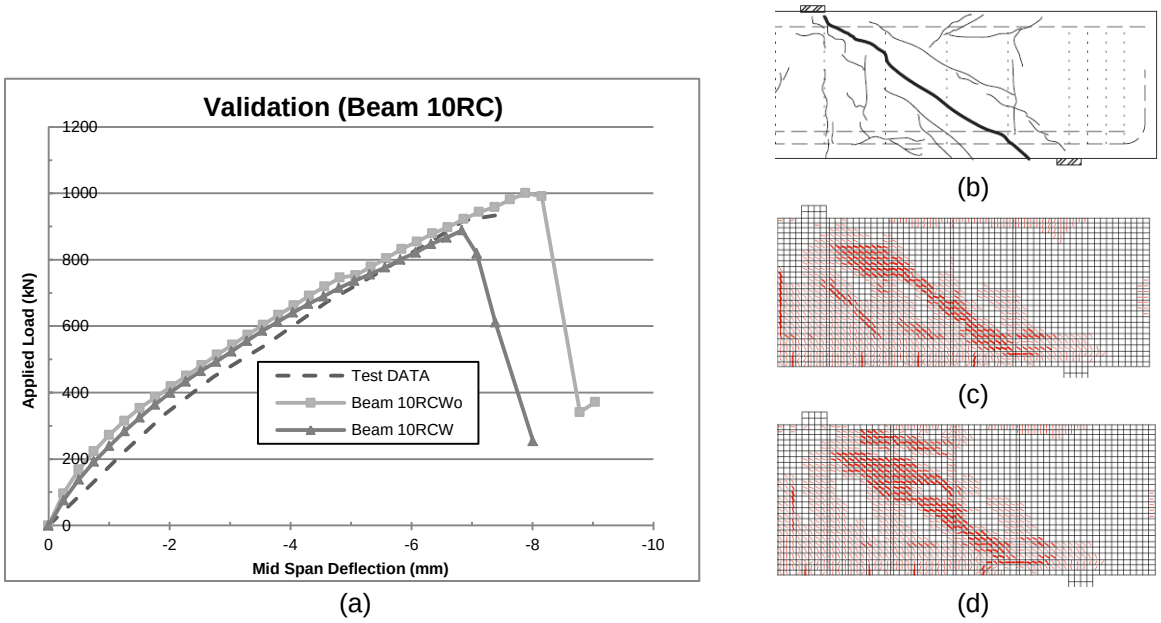

Figure 8: (a) Load-deflection for **Moderate** corrosion levels; (b) Crack map at failure for test specimen (Higgins et al. 2003); (c) Crack prediction **without** pre-straining; (d) Crack prediction **with** pre-straining

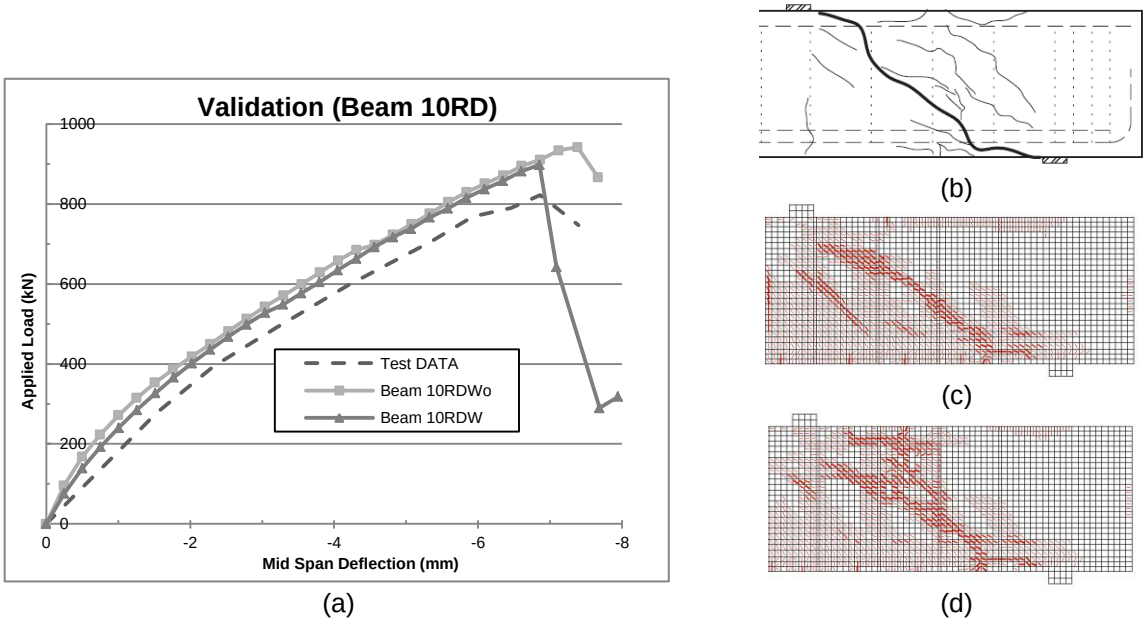

Figure 9: (a) Load-deflection for **High** corrosion levels; (b) Crack map at failure for test specimen (Higgins et al. 2003); (c) Crack prediction **without** pre-straining; (d) Crack prediction **with** pre-straining

5. Conclusions

From the finite element results presented in this paper, the following conclusions can be drawn:

1. The LS elements successfully model shear critical members and provide good agreement with published data.
2. Corrosion steel loss and corrosion-induced cracking are successfully introduced within a two-dimensional plane-stress problem.
3. The use of LS elements with the cracking model also provides good agreement with published data.
4. Corrosion-induced cracking in terms of pre-straining becomes more effective at higher levels of corrosion and better reproduces the induced damage at failure.

As part of ongoing work, the finite element model is being used in a parametric analysis to identify critical variables/mechanisms to account in the shear capacity assessment of reinforced concrete flexural members affected by corrosion of the steel stirrups.

6. Acknowledgements

Financial support through the Natural Sciences and Engineering Research Council of Canada (NSERC), the Queen Elizabeth II Graduate Scholarship in Science and Technology, and the University of Ottawa Admission Scholarship is gratefully acknowledged.

7. References

Hanjari, K.Z., Kettil, P. and Lundgren, K. .2011. Analysis of Mechanical Behavior of Corroded Reinforced Concrete Structures. *ACI Structural Journal*, **108**(5).

Higgins, C., Farrow III, W.C., Potisuk, T., Miller, T.H. and Yim, S.C. .2003. *Shear Capacity Assessment of Corrosion-Damaged Reinforced Concrete Beams*, Department of Civil Engineering, Oregon State University, Oregon Department of Transportation Research Unit, 200 Hawthorne Ave. SE, Suite B-240, Salem OR, 94301-5192 and Federal Highway Administration, 400 Seventh S. W., Washington DC 20590.

Martín-Pérez, B. 1999. *Service Life Modelling of R.C. Highway Structures Exposed to Chlorides*. Department of Civil Engineering. Toronto, Canada, University of Toronto: 168 pp.

Miller, T.H., Potisuk, T., Higgins, C.C. and Yim, S.C. .2011. Finite element analysis of reinforced concrete beams with corrosion subjected to shear. *Advances in Civil Engineering*, **2011**.

Rosenberg, A., Hansson, C.M. and Andrade, C. 1989. Mechanisms of corrosion of steel in concrete. *Materials Science of Concrete I.* J. Skalny. Westerville, OH: 285-313.

Vecchio, F.J. 2000. Analysis of shear-critical reinforced concrete beams. *ACI Structural Journal*, **97**(1), 102-110.

Vecchio, F.J. 2000. Disturbed stress field model for reinforced concrete: Formulation. *Journal of Structural Engineering*, **126**(9).

Vecchio, F.J., Lai, D., Shim, W. and Ng, J. 2001. Disturbed stress field model for reinforced concrete: validation. *Journal of Structural Engineering*, **127**(4).

Wong, P.S. and Vecchio, F.J. 2002. *VecTor2 & Formworks User's Manual*. University of Toronto.